Electronic Supplementary Information

An Oriented, Siliceous Deca-dodecasil 3R (DDR) Zeolite Film for Effective Carbon Capture: Insight into Its Hydrophobic Effect

Eunjoo Kim,[1] Sungwon Hong,[1] Eunhee Jang,[1] Jeong Hyeon Lee,[2] Jin Chul Kim,[2] Nakwon Choi,[3] Churl Hee Cho,[4] Jaewook Nam,[5] Sang Kyu Kwak,[2] Alex C.K. Yip,[6] and Jungkyu Choi[1,*]

[1] Department of Chemical & Biological Engineering, College of Engineering, Korea University (KU), 145 Anam-Ro, Seongbuk-gu, Seoul 02841, Republic of Korea

[2] School of Energy and Chemical Engineering, Ulsan National Institute of Science and Technology (UNIST), Ulsan 44919, Republic of Korea

[3] Center for BioMicrosystems, Brain Science Institute, Korea Institute of Science and Technology (KIST), 5 Hwarang-ro 14-gil, Seongbuk-gu, Seoul 02792, Republic of Korea

[4] Graduate School of Energy Science & Technology (GEST), Chungnam National University (CNU), 99 Daehak-ro, Yuseong-gu, Daejeon 34134, Republic of Korea

[5] School of Chemical Engineering, Sungkyunkwan University, Suwon 16419, Republic of Korea.

[6] Department of Chemical and Process Engineering, University of Canterbury, Christchurch, New Zealand

* Corresponding Author

E-mail address: jungkyu_choi@korea.ac.kr, Phone: +82-2-3290-4854, and Fax: +82-2-926-6102

Experimental

Synthesis of DDR zeolite particles

DDR seed crystals were first synthesized by using non-seeded growth based on a procedure reported elsewhere with a minor difference being the use of LUDOX® HS-40 colloidal silica (40 wt% suspension in H_2O, Sigma-Aldrich).[1] The resulting seed crystals were then used to synthesize mono-dispersed Si-DDR particles (~3 μm). Specifically, 1-adamantylamine (ADA, 97%, Sigma-Aldrich) was dissolved in ethylenediamine (EDA, 98%, Sigma-Aldrich) by shaking a round flask for 1 h with a shaking machine (Lab Companion, SI-300R, South Korea) and subsequently sonicating the flask for 1 h. The solution was then added to deionized (DI) water, followed by adding a silica source of CAB-O-SIL (Cabot Corporation, M5 grade). The flask was placed in a silicon oil bath, which was heated to 95 ℃, and was further stirred for 1 h. The final molar composition of a synthesis precursor was 9 ADA:150 EDA:100 SiO_2:4,000 H_2O. After cooling to room temperature, ~0.1 g of the aforementioned Si-DDR particles were added to the prepared synthesis precursor and the final precursor was transferred to a Teflon liner. The Teflon liner was mounted in an autoclave and the autoclave was placed in a rack for rotation in an oven, which had been pre-heated to 160 ℃. After 4 d of synthesis, the reaction was quenched by tap water. After that, solid particles were recovered by vacuum filtration and washed with copious DI water.

Si-DDR particles with a size of ~820 nm were finally synthesized by modifying a previously reported method.[2] First, 1 g of the recovered DDR particles with the size of ~3 μm was ball-milled at 300 rpm for 12 h. Then, a DDR seed suspension was prepared by adding ~1 g of the ball-milled DDR particles to ~1 L of DI water. In parallel, ~20 g of a DDR synthetic precursor, which contained ADA, AS-30 (LUDOX® AS-30 colloidal silica; 30 wt% suspension in H_2O, Sigma-Aldrich), EDA, and H_2O at the molar ratios of 6:100:50:10,000, respectively, were prepared. Subsequently, ~10 g of the DDR seed suspension was added to the DDR synthetic precursor and the mixture was further mixed overnight using the shaking machine. After mixing homogeneously, ~30 g of the final mixture was poured into a Teflon liner (~50 mL) and reacted hydrothermally at 160 ℃ for 4 d. The resulting powder was collected through centrifugation and washed with DI water. This step was repeated at least three times. The recovered powder was further calcined at 550 ˚C for 12 h at a ramp rate of 1 ℃·min^{-1} under an air flow of 200 mL·min^{-1}.

Formation of a DDR seed layer

To achieve our overarching goal of using zeolite membranes for industrial applications at a scale as large as the post-combustion carbon capture process in a coal-fired power plant, the establishment of simple, yet robust methods for seed layer formation and subsequent reliable secondary growth is critical. For this purpose, a simple, inexpensive dip-coating method was adopted in this study for forming a continuous DDR seed layer. About 0.05 g of calcined DDR particles was added to ~40 mL ethanol and the suspension was sonicated. Next, this DDR dispersion was brought in contact with a polished side of an α-alumina disc (~20 mm in diameter and ~2 mm in thickness) for ~30 s. The disc was then taken out slowly and allowed to dry for 30 s. This process was repeated four times. The seeded α-Al_2O_3 disc was calcined under an ambient condition by heating to 450 ℃ with a ramp rate of 1 ℃·min^{-1} and remained soaked at 450 ℃ for 4 h. During the calcination step, air flow at ~200 mL·min^{-1} was fed continuously to a furnace. Although a more uniform seed layer without the empty region can be obtained via chemical deposition[3, 4] or sonication-assisted deposition,[5-7] the simple dip-coating method adopted here is highly desirable for the ease of scaling up the DDR zeolite membranes.

Synthesis of DDR films

Continuous DDR films were fabricated by conducting hydrothermal growth of the seeded α-Al_2O_3 disc. Methyltropinium iodide (MTI) as a SDA was required to synthesize ZSM-58.[8, 9] To synthesize MTI, 50 g of iodomethane (99%, Sigma-Aldrich) was dissolved in 200 mL of ethanol and stirred for 30 min. After this solution became clear, 50 g of tropine (98%, Alfa Aesar) was added and refluxed further at room temperature for 3 d in a dark environment by wrapping the entire round flask with aluminium foil. After completion of the reaction, white powder was collected by filtration with ethanol and dried at ~80 $^{\circ}$C prior to use in the secondary growth of a DDR seed layer.

A synthetic precursor for secondary growth was prepared by adding a silica suspension (LUDOX HS-40; 40 wt% suspension in H_2O, Sigma-Aldrich) as well as the organic template of MTI to DI water. This precursor was further mixed by using the shaker for 1 h. Subsequently, NaOH (98% pellets, Sigma-Aldrich) was added and the resulting synthetic precursor was mixed well overnight in the shaking machine. The prepared precursor was opaque immediately after the addition of NaOH, but overnight shaking rendered it transparent. The final molar composition of the ZSM-58 precursor was 100 SiO_2:25 MTI:30 NaOH:4000 H_2O. The precursor was poured into a Teflon liner into which a seeded α-Al_2O_3 disc was tilted with the seeded side facing down. The Teflon liner was then mounted into an autoclave and the

autoclave was placed in a pre-heated oven at 130 ℃. The hydrothermal treatment for secondary growth was conducted for 2, 4, 6, 8, 10, and 15 d. After the reaction in the autoclave was quenched with tap water, a DDR type film was recovered and dried at room temperature. Subsequently, the sample was calcined at 550 ℃ for 12 h at a ramp rate of 0.5 ℃·min^{-1} under air flow at 200 mL·min^{-1}. The resulting film or membrane is referred to as DZ_xd, where D indicates the DDR seed layer, Z represents the synthesis of ZSM-58 adopted for the secondary growth, and x stands for the varied hydrothermal reaction time in d: 2, 4, 6, 8, 10, and 15. Although ZSM-58 particles themselves are not appropriate for constituting a uniform seed layer, our synthetic route toward ZSM-58 was adopted to inter-grow a Si-DDR seed layer toward the continuous DDR film.

Membrane characterizations

Scanning electron microscopy (SEM) images were acquired with a Hitachi S-4300 instrument. Surfaces of all samples were Pt-sputtered prior to imaging. In addition, X-ray diffraction (XRD) patterns were obtained using a Rigaku Model D/Max-2500V/PC diffractometer (Japan) with Cu K_α radiation (λ = 0.154 nm). A crystallographic information file (CIF), downloaded from the International Zeolite Association (IZA) website, was processed to acquire the simulated XRD pattern of Si-DDR zeolites. For processing, the Mercury software (available from the Cambridge Crystallographic Data Centre; CCDC) was used. Crystallographic preferential orientation (CPO) values of the (101) plane were calculated by using a following formula:

$$\mathrm{CPO}_{(101)/x} = \left[I_{(101)} / I_x\big|_M - I_{(101)} / I_x\big|_P \right] / \left(I_{(101)} / I_x\big|_P \right),$$

where subscripts of *P* and *M* denote the DDR powder and membrane, respectively. In order to quantify the degree of the *h0h*-out-of plane orientation of the DDR membranes, we compared the XRD intensities of the (101) reflections with those of $(2\bar{1}3)$ and (104) reflections, which served as references (here indicated by the placeholder *x*). Fluorescence confocal optical microscopy (FCOM) images of the dye-saturated DDR membranes were obtained by using a Carl Zeiss LSM 700 confocal microscope equipped with a solid state laser (wavelength: 555 nm). The DDR membranes were impregnated with fluorescent dye molecules using "osmosis-type" module.[10] The membrane side (i.e., α-Al_2O_3 disc top) was contacted with 1 mM fluorescein sodium solution (Sigma-Aldrich), while the opposite side (i.e., α-Al_2O_3 disc bottom), was contacted with DI water. Dyeing duration was ~4 d. The size of fluorescein molecules (~0.9 nm) is smaller than that of intercrystalline defects, but larger than that of DDR zeolitic pores (~0.4 nm), allowing for the selective dyeing of defects.

The CO_2/N_2 separation performance of the DDR membranes was measured using the custom-made permeation system described in our previous study.[11] The Wicke-Kallenbach mode was used; both the feed and permeate sides were maintained at a total pressure of ~1 atm. The partial pressures of CO_2 and N_2 in the feed under the dry condition were 50.5 kPa and 50.5 kPa, respectively (referred to as 50:50 DRY), while those of CO_2, N_2, and H_2O under the wet condition were 49 kPa, 49 kPa, and 3 kPa, respectively (50:50 WET). In addition, simulated flue-gas mixtures, composed of 15.2 kPa CO_2 and 85.9 kPa N_2 (referred to as 15:85 DRY) and 14.7 kPa CO_2, 83.3 kPa N_2, and 3 kPa H_2O (referred to as 15:85 WET) were used as feed. In summary, a total flow rate (dry basis) of ~100 mL·min^{-1} was used to provide the feed mixture and the helium flow rate of ~100 mL·min^{-1} was used for sweeping. In addition, we used the total flow rates (dry basis) of ~50 and ~200 mL·min^{-1} for testing the CO_2/N_2 separation performance of membrane DZ_10d. The permeating species on the permeate side was further sent to a gas chromatograph (YL 6100 GC, YOUNG LIN, South Korea) equipped with a packed column (6 ft × 1/8" Propak T) and a thermal conductivity detector (TCD) for on-line analysis. For reliable analyses, CH_4 was added to the permeate flow for use as the internal standard.

Theory

Grand canonical Monte Carlo simulation

We modeled the periodic crystal structure of DDR zeolites (Fig. S13a) and performed a grand canonical Monte Carlo (GCMC) simulation to elucidate the adsorption behaviors of guest molecules in the DDR zeolite. We used a Sorption program[12] to estimate the average adsorbed amounts of CO_2 and N_2 molecules in the presence and absence of H_2O via the GCMC simulation. The GCMC simulations of 5×10^6 equilibrium and 5×10^6 production steps were independently performed five times to obtain the amounts of the adsorbed molecules. Considering the careful consideration of inaccessible pockets in the zeolite that Krishna et al.[13] emphasized in a previous study, we assumed that these pockets were blocked by inactive atoms, which were not involved in energy calculations. Rigid molecular models of CO_2, N_2, and H_2O, which correspond to 3LJ3CB.EPM2,[14] 2LJ3CB.MSKM,[15, 16] and TIP3P,[17] respectively, were used. The bond lengths of C–O in CO_2, N–N in N_2, O–H in H_2O were kept constant at 1.16 Å, 1.098 Å, and 0.9572 Å, respectively. These models have been shown to be effective for estimating the adsorption isotherm in various zeolites.[13, 18-21] Coulombic and Lennard-Jones parameters for silanol groups were procured from the CLAYFF[22] force field and the partial charge of the hydrogen atoms was adjusted for the charge neutrality in the periodic cell. The potential energy parameters between the guest molecules and the zeolite were optimized to reproduce the experimental adsorption isotherm (Fig. S14). Detailed

information on potential parameters and partial charges relevant to the simulations is summarized in Table S1.

The simulated adsorption isotherms of CO_2 and N_2 single components were in good agreement with the experimental data in the literature,[1, 13, 18-20, 23, 24] validating simulation approaches in this study (Fig. S14a). For water adsorption, however, it appears that the simulation data reported in previous studies[21, 25, 26] underestimated the adsorbed amount in low pressure regions, as internal defects were not appropriately considered. Most siliceous zeolites would have intrinsic siloxy ($–O_3–Si–O^-$) defects during synthesis, which become silanol groups after calcinations.[27] These silanol groups are known to promote water condensation at low pressure and thus, increase its adsorption amount.[28, 29] In our previous study,[1] the ^{29}Si MAS NMR characterization revealed the presence of ~1.5% silanol defects in Si-DDR zeolites and this degree was assumed in creating the framework model for GCMC simulations. Considering that a defective Si atom can generate four silanol defects in total and that there are 120 Si atoms in the unit cell of a DDR zeolite, three defective Si atoms (i.e., 12 silanol nest defects) were introduced to maintain 1.5% defects in a 2 × 4 × 1 supercell of the DDR zeolite. The simulated adsorption isotherm of H_2O was considerably comparable to the experimental counterpart (Fig. S14b).

Furthermore, we conducted GCMC simulation with a slab model, where the *z*-axis was perpendicular to the (101) plane with a 10 nm vacuum region on the both sides, while the outer surface was terminated by silanol groups (Fig. S13b). This simulation was carried out mainly to observe the adsorption properties of H_2O molecules on the outer surface. Thus, the silanol nest defects, considered in the model in Fig. S13a, were not considered. The lattice parameters of the porous crystal structure in the slab model were 47.419 × 41.580 × 146.585 ($Å^3$) with a tilted γ angle of 63.995°.

Density functional theory calculation

To investigate entrance effects on the diffusion of guest molecules at the zeolite surface with and without the water-solvated condition, two cage-shaped cluster models of zeolite surface were considered. To represent the surface structure with the effect of the hydroxyl group, the 46T and 48T cluster models, which contained a whole dtr cage ($4^3 5^{12} 6^1 8^3$) with some portion of det ($4^3 5^6 6^1$) and red (5^{12}) cages, were acquired through the partial optimization procedure[30, 31] in the DMol^3 program.[32, 33] We employed the PBE exchange-correlation function and the DNP 4.4 basis set with the all-electron relativistic core treatment. The convergence criteria for energy, force, and displacement were set to 1×10^{-5} Ha, 0.002 Ha/Å, and 0.005 Å, respectively. To include the dispersion correction of the van der Waals effect, the Tkatchenko-

Scheffler scheme[34] was used. The COSMO solvation model[35] was applied to describe the water environment of the wet condition. Several plausible configurations of guest molecules near the zeolite surface were sampled and the most stable configuration was used for the comparison of the systems under the dry and wet conditions.

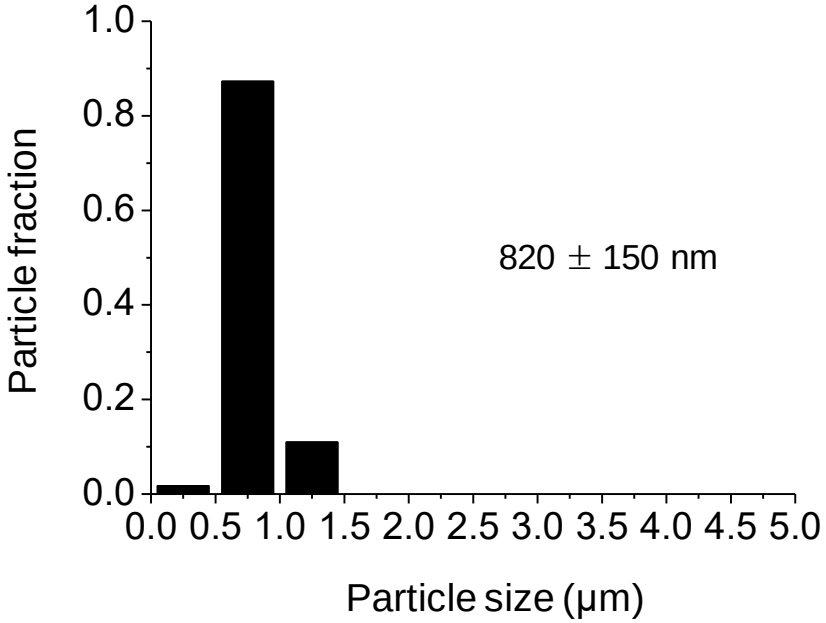

Fig. S1. Size distribution of the particles shown in Fig. 1a. The particle size is measured along the longest direction in the diamond-like basal plane. The resulting average size and its standard deviation are given.

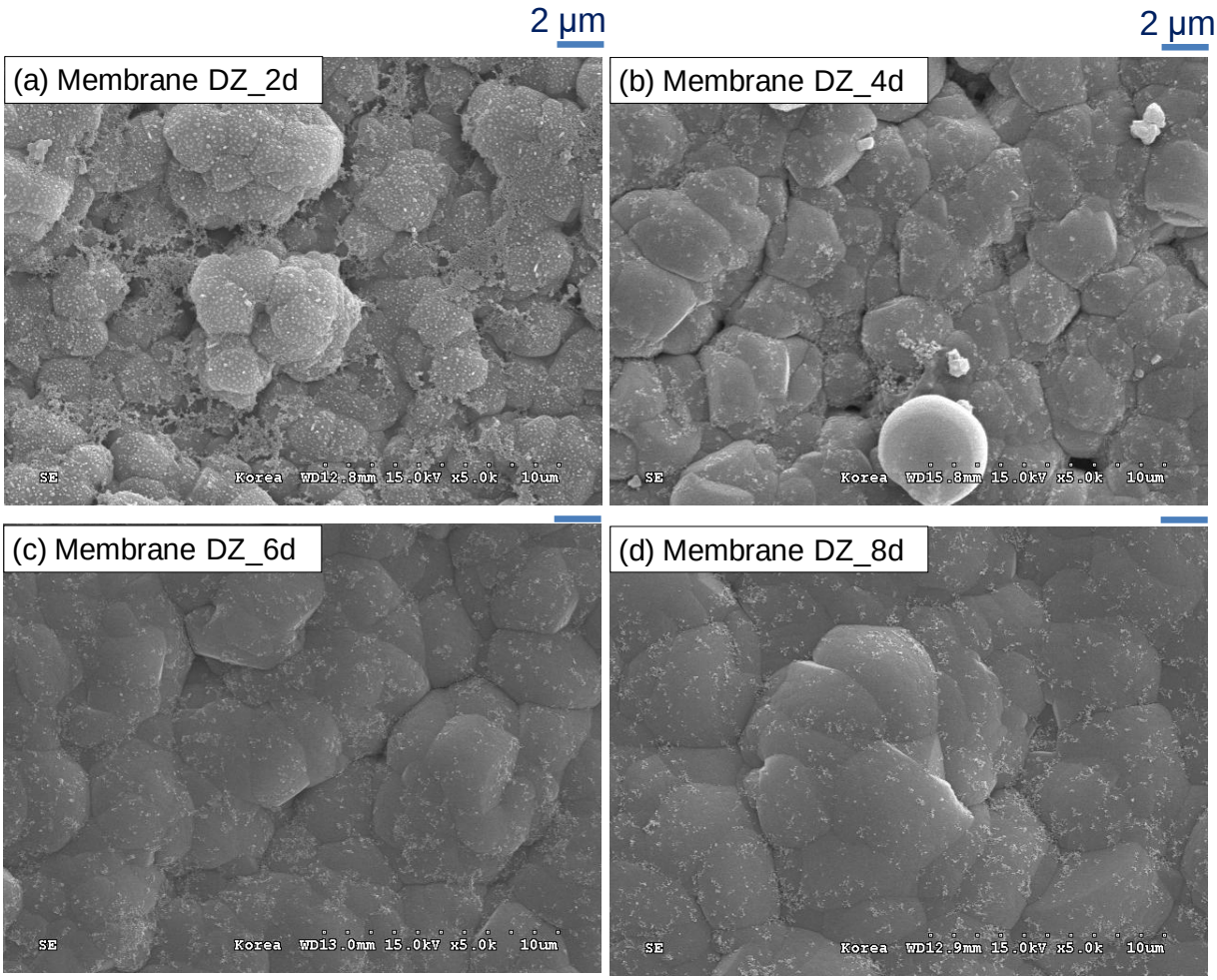

Fig. S2. Top-view SEM images of membranes (a) DZ_2d, (b) DZ_4d, (c) DZ_6d, and (d) DZ_8d. All scale bars represent 2 μm.

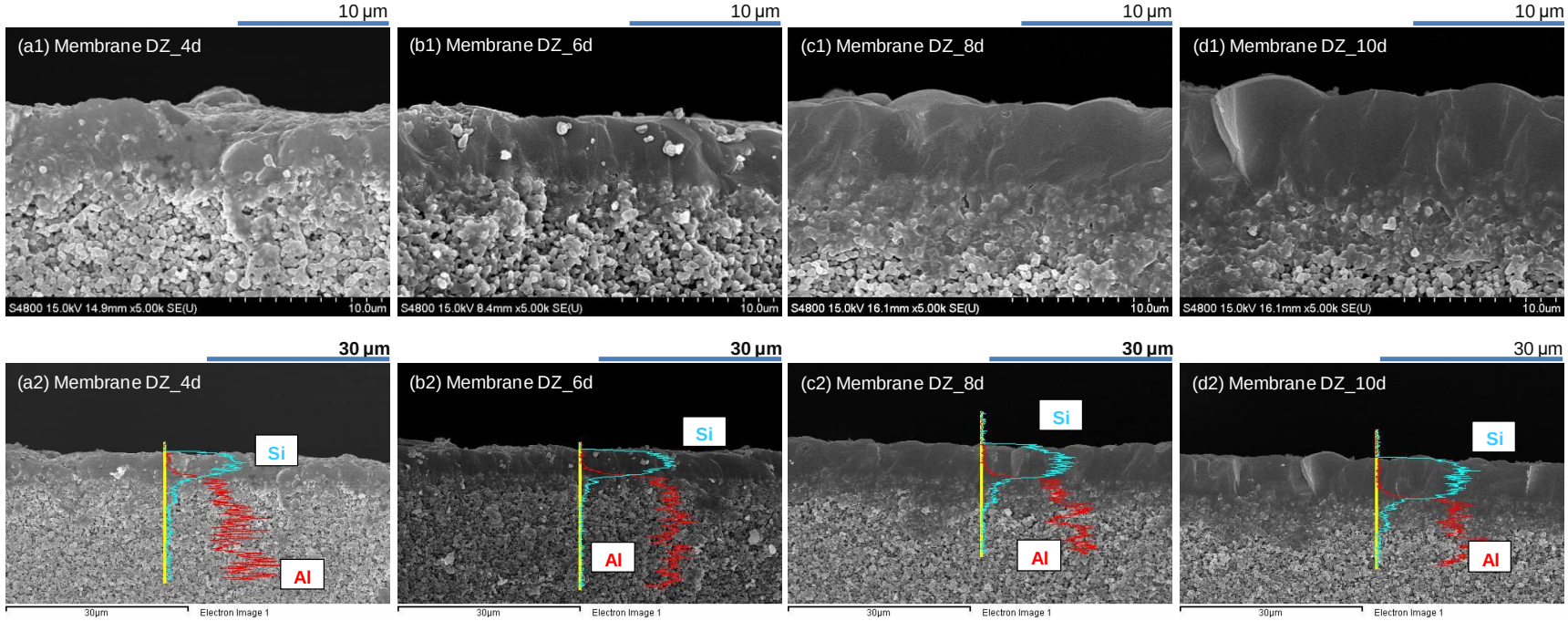

Fig. S3. Cross-sectional SEM images (*top*) and EDX results (*bottom*) of membranes (a1)-(a2) DZ_4d, (b1)-(b2) DZ_6d, (c1)-(c2) DZ_8d, and (d1)-(d2) DZ_10d.

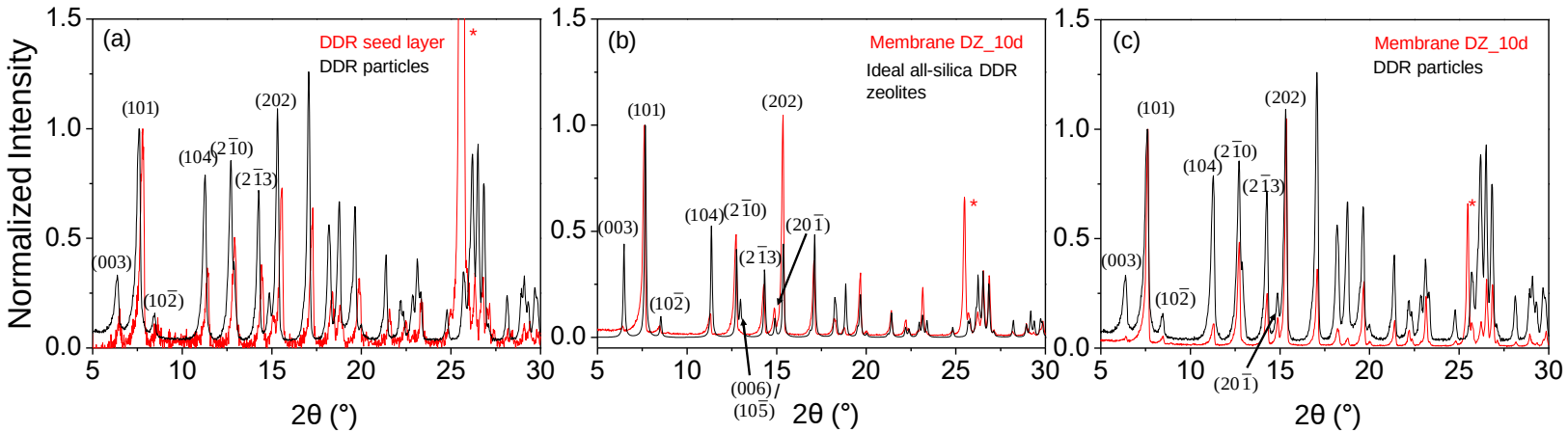

Fig. S4. XRD patterns of (a) a DDR seed layer (the unlevel background was corrected) and DDR particles, (b) membrane DZ_10d and an ideal all-silica DDR zeolite structure (acquired from the crystallographic information file, which was downloaded from the International Zeolite Association website), and (c) membrane DZ_10d and DDR particles. The asterisk (*) indicates an XRD peak from the α-Al_2O_3 disc.

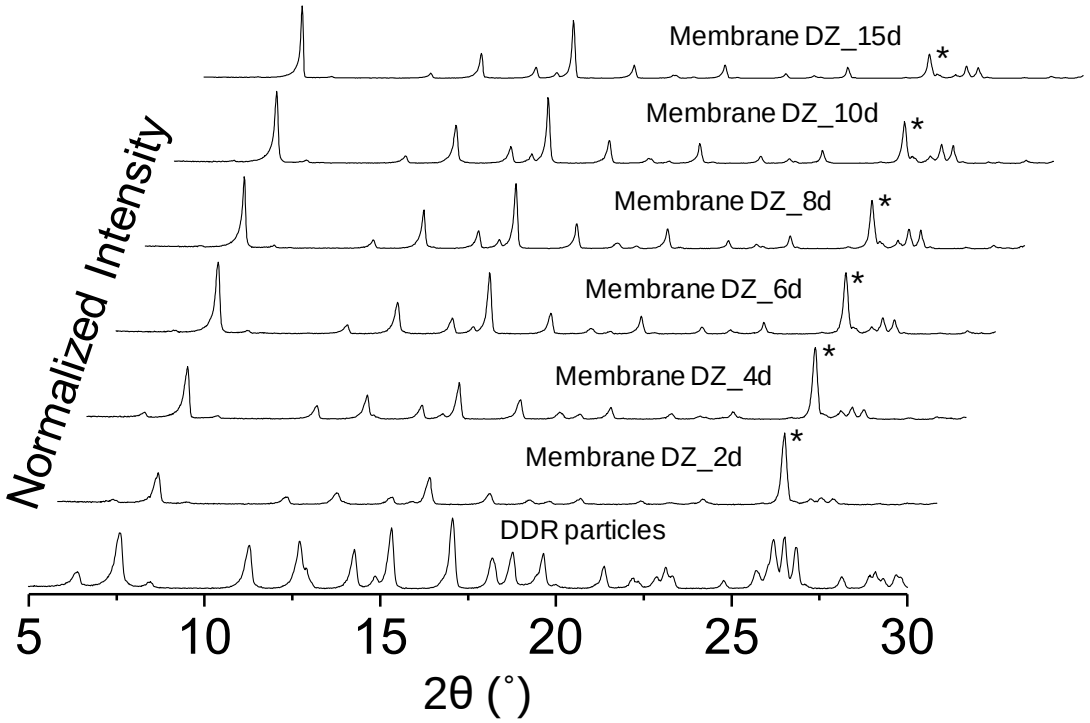

Fig. S5. XRD patterns of membranes DZ_xd (x = 2, 4, 6, 8, 10, and 15). In addition, the XRD pattern of Si-DDR particles is added as a reference and the asterisks (*) indicate the XRD peak from the α-Al_2O_3 disc.

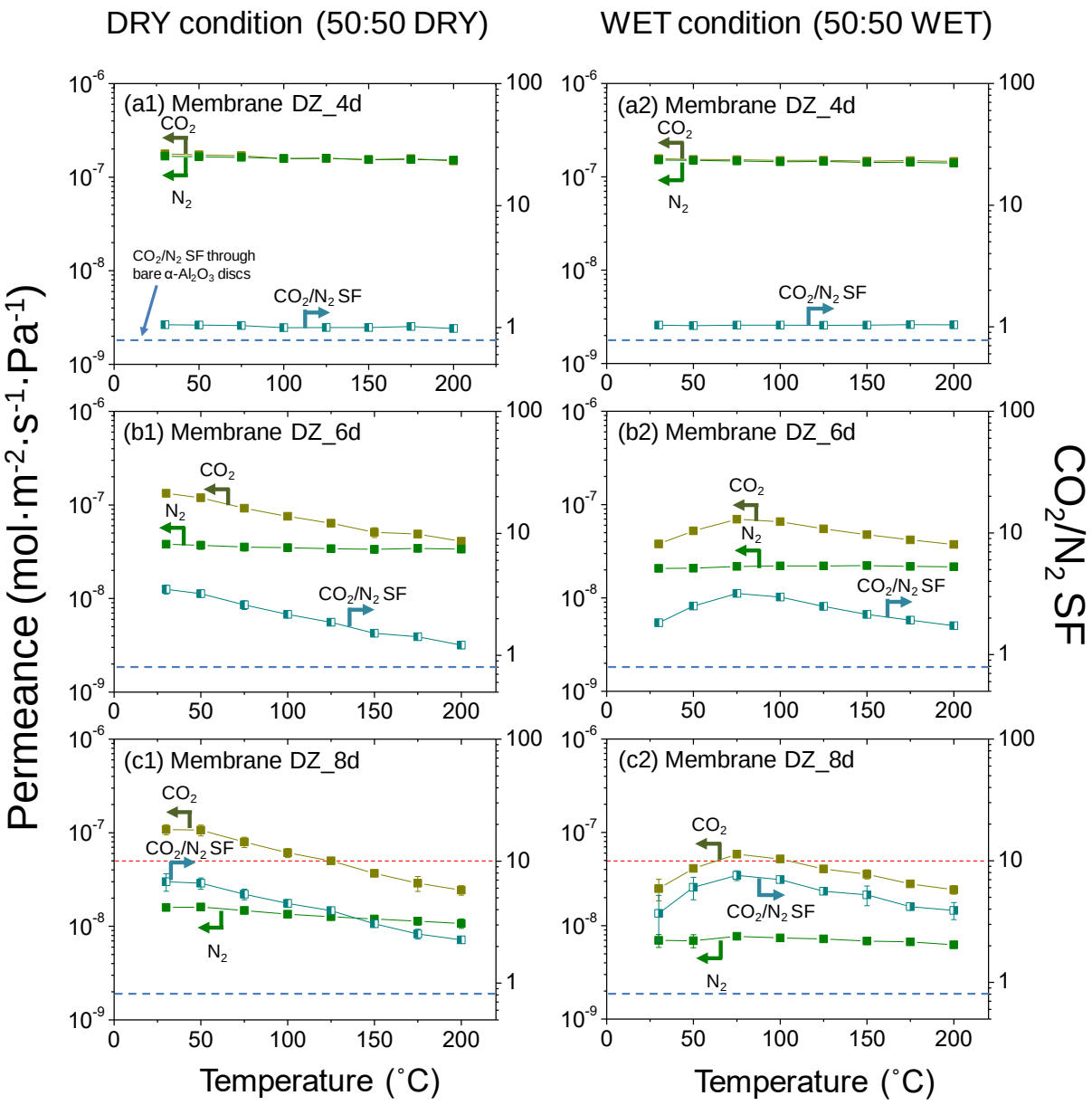

Fig. S6. Permeances of CO_2 and N_2 and their corresponding CO_2/N_2 SFs through membranes (a1)-(a2) DZ_4d, (b1)-(b2) DZ_6d, and (c1)-(c2) DZ_8d as a function of temperature (up to ~200 ℃) under the dry (50:50 DRY) and wet (50:50 WET) conditions. The blue dashed lines that indicate the CO_2/N_2 SF through a bare α-Al_2O_3 disc are included for comparison. In addition, in (c1)-(c2), the red dashed lines that illustrate the CO_2/N_2 SF of 10 are included for comparison.

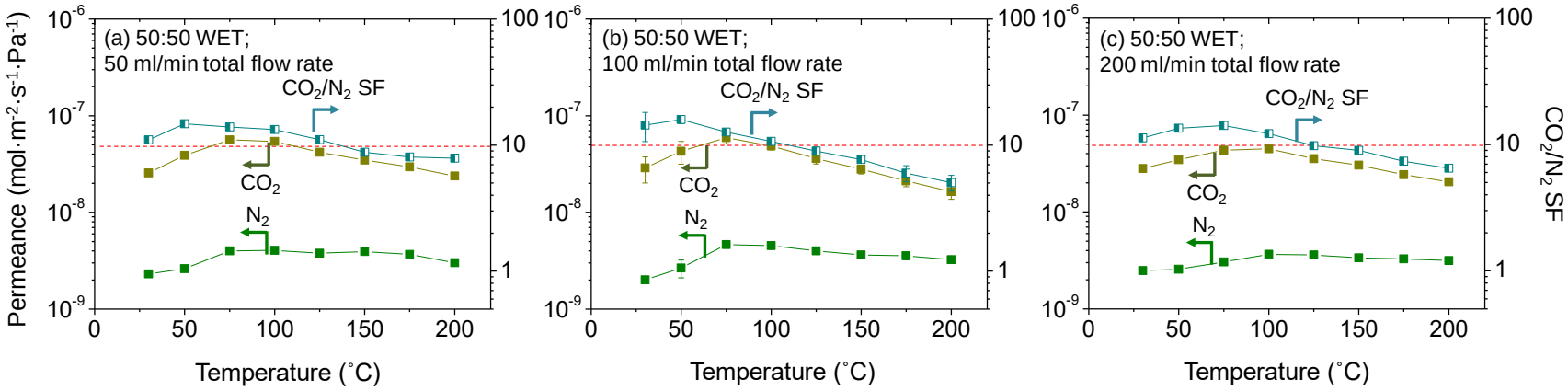

Fig. S7. Permeances of CO_2 and N_2 and their corresponding CO_2/N_2 SFs through membrane DZ_10d under the wet condition (50:50 WET) by varying the total feed volumetric flow rates (dry basis): (a) 50 mL·min^{-1}, (b) 100 mL·min^{-1} (identical to the graph shown in Fig. 2b), and (c) 200 mL·min^{-1}. For better comparison, the red dashed lines that represent the CO_2/N_2 SF of ~10 are added in (a)-(c).

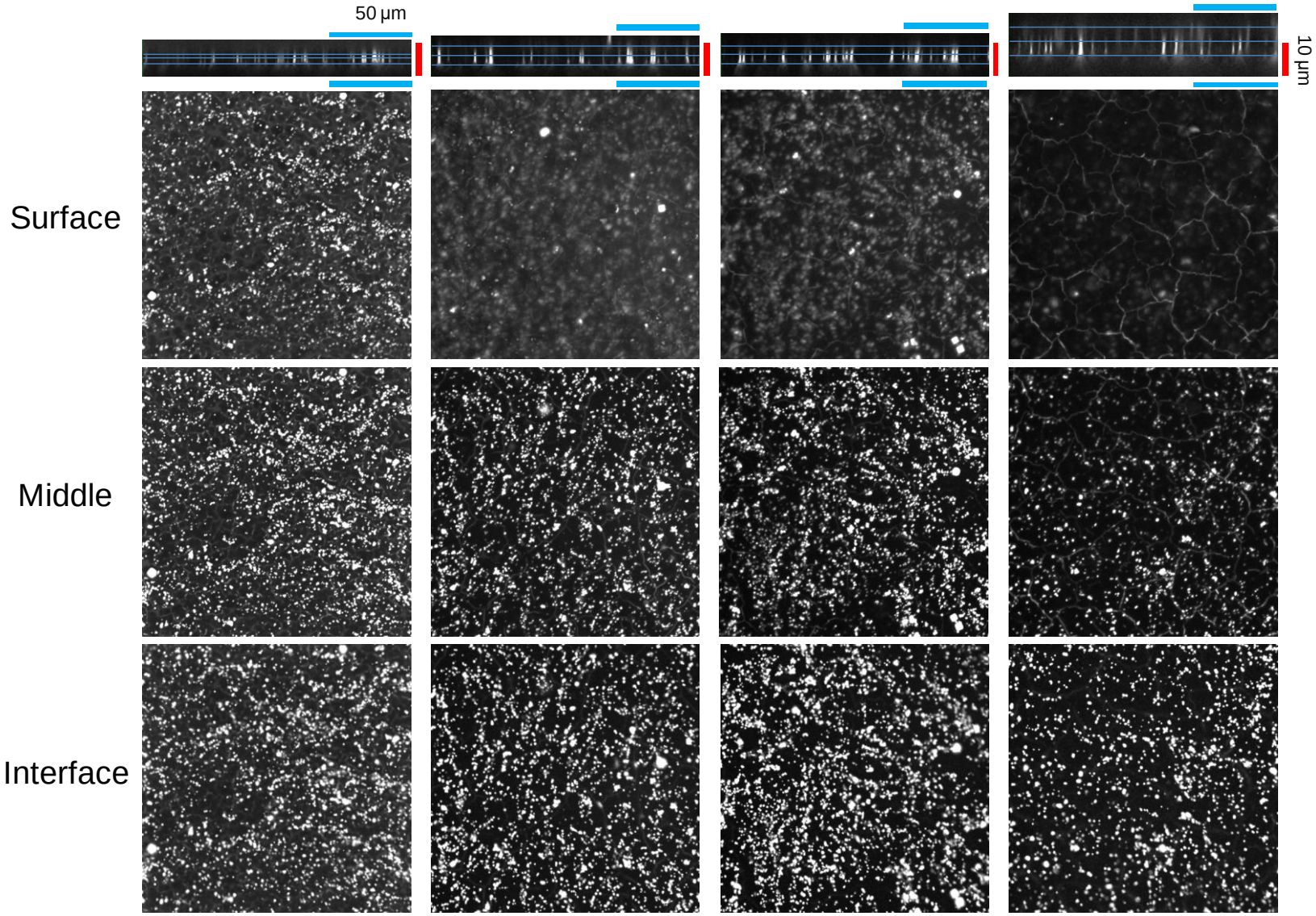

Fig. S8. Cross-sectional-view FCOM images (*1st row*) and top-view FCOM images (*2nd-4th row*) obtained at the positions of lines for membranes DZ_4d (*1st column*), DZ_6d (*2nd column*), DZ_8d (*3rd column*), and DZ_10d (*4th column*).

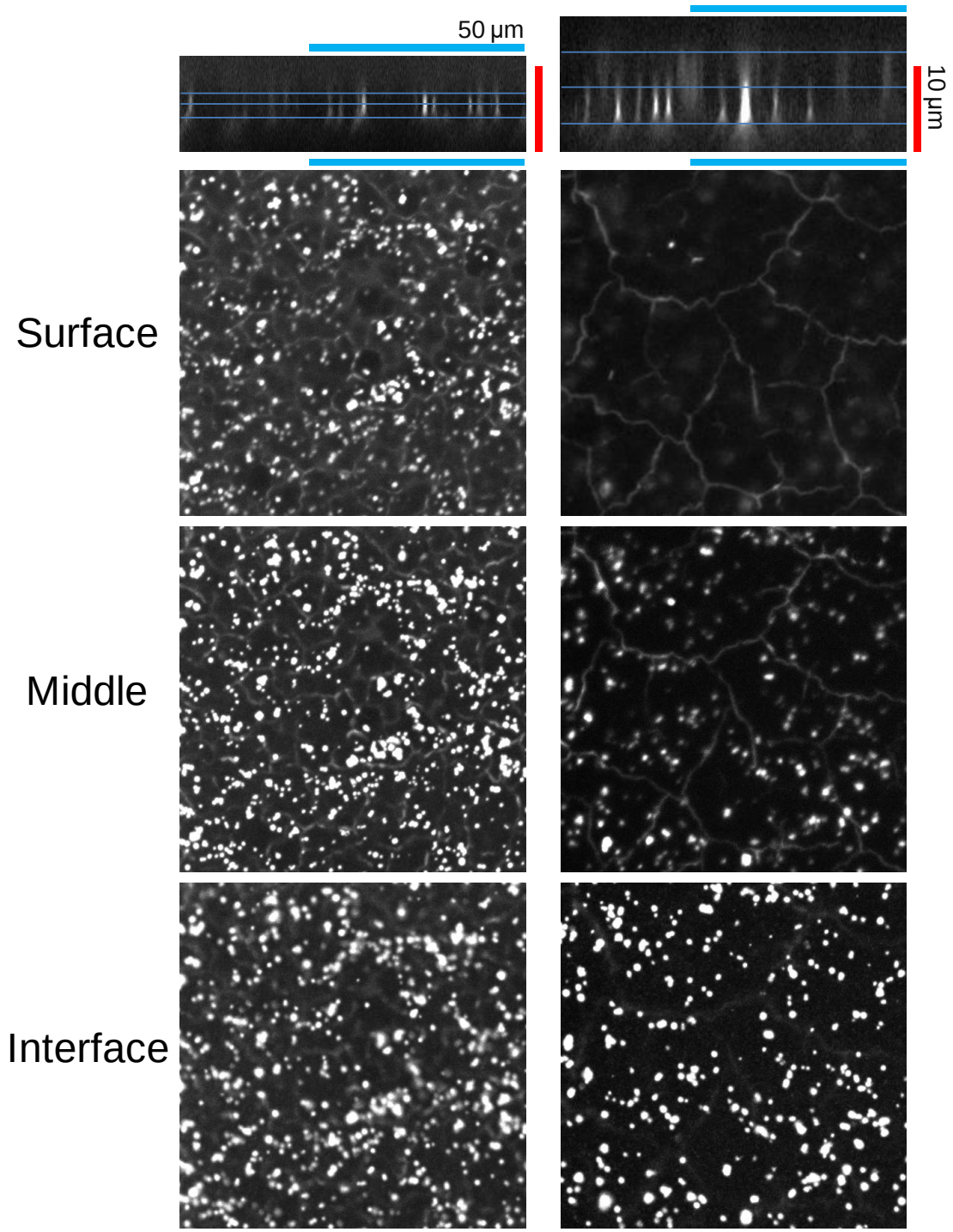

Fig. S9. Cross-sectional-view and top-view FCOM images of membranes DZ_4d (*left*) and DZ_10d (*right*) at a higher magnification, as compared with those in Fig. S8. For the top-view FCOM images (2^{nd}-4^{th} *rows*), the positions where the FCOM images were obtained are designated in the corresponding cross-sectional-view FCOM images (1^{st} *row*).

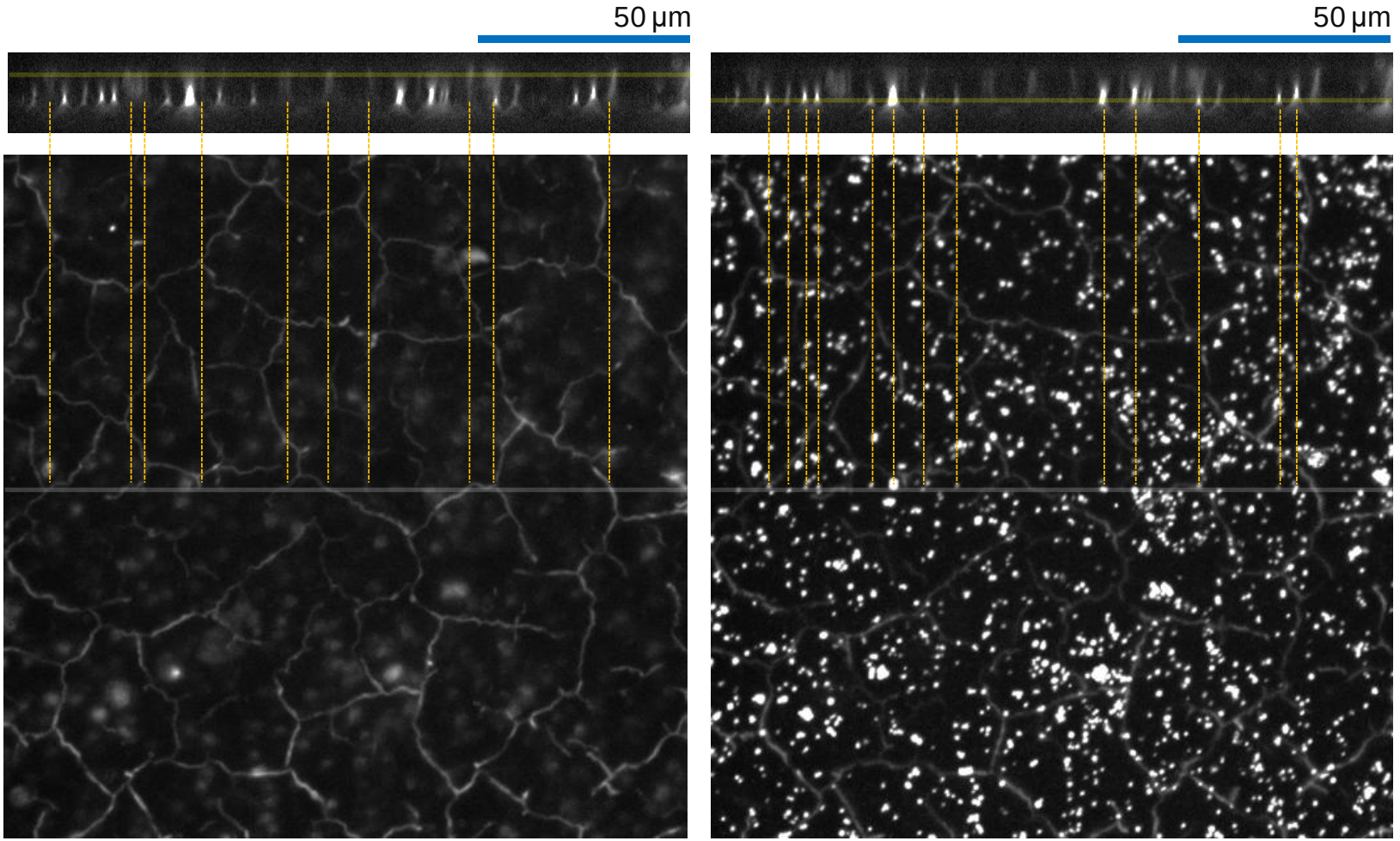

Fig. S10. Cross-sectional-view FCOM images of membrane DZ_10d (*top*) were obtained along the middle translucent white lines on the top-view FCOM images (*bottom*) together with other slices. The top-view FCOM images of membrane DZ_10d (*bottom*) were obtained at the position designated by the translucent yellow lines in the cross-sectional FCOM images (*top*). The yellow dashed lines on the top-view FCOM images indicate cracks (*left*) and cavities (*right*) and are further associated with the defect features in the cross-sectional FCOM images (*top*).

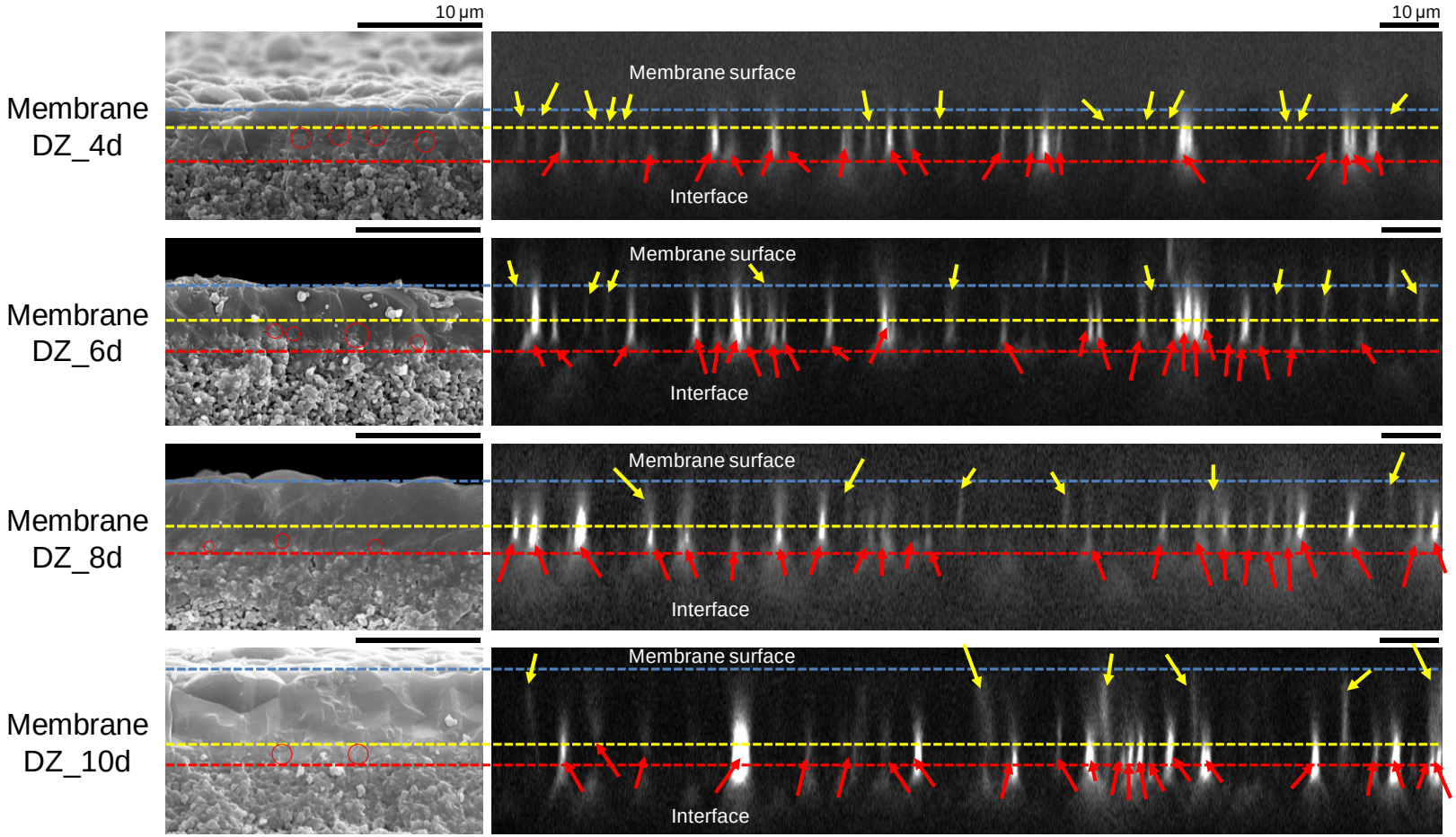

Fig. S11. Cross-sectional-view SEM images (*left*) and FCOM images (*right*) of membranes DZ_4d (1^{st} *row*), DZ_6d (2^{nd} *row*), DZ_8d (3^{rd} *row*), and DZ_10d (4^{th} *row*). The blue and red dashed lines were added to designate the membrane surface and interface, respectively, while the yellow dashed lines were used to approximate the position below which apparent defective cavities were present. For visual guidance, the yellow and red arrows are used to indicate the cracks (propagating down to the interface) and cavities (primarily present below the yellow dashed lines), respectively. The cavities observed in the SEM images are marked by red circles. The black scale bars represent 10 µm.

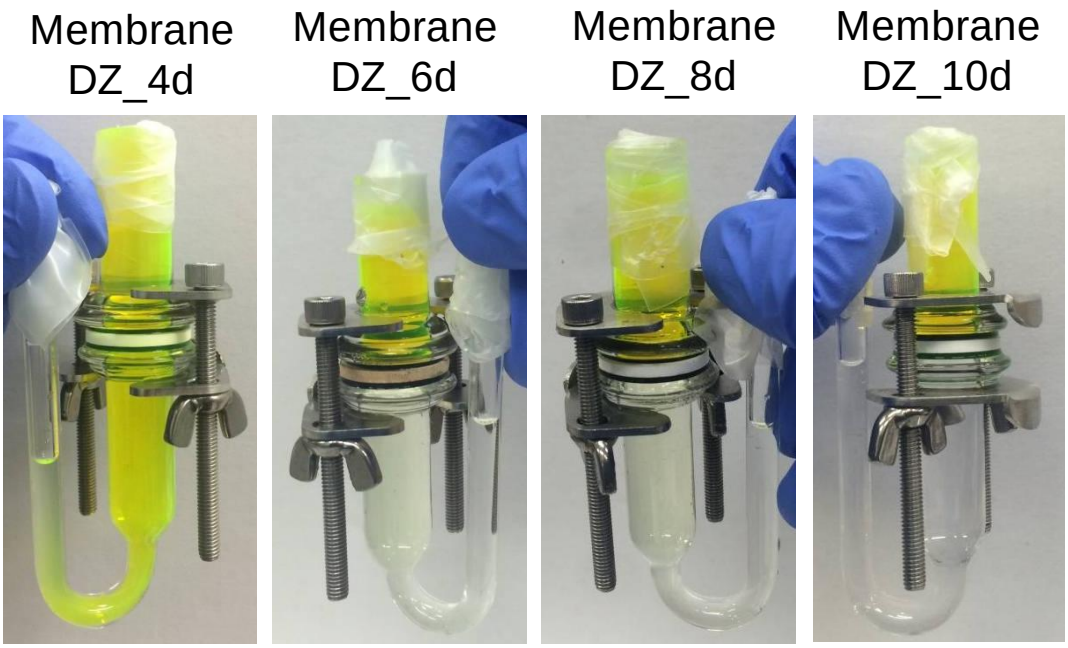

Fig. S12. Pictures taken after conducting the dyeing of membranes DZ_4d, _6d, _8d, and _10d for 4 d. The lower part of the dyeing module qualitatively indicates a degree of the dye molecules that passed through the DDR membranes and thus, the density and/or size of defects.

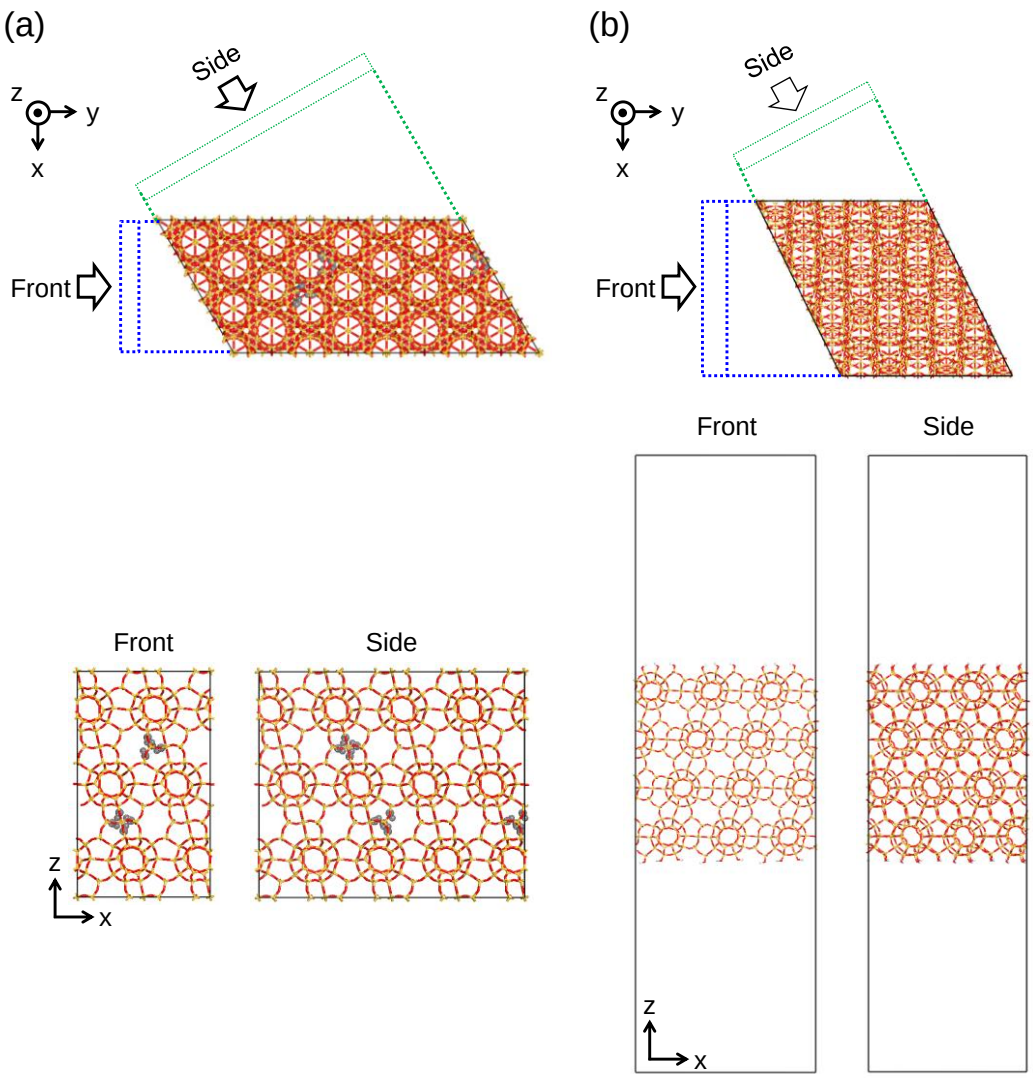

Fig. S13. (a) Periodic crystal model of 2 × 4 × 1 supercell of DDR zeolites. OH groups, indicated by grey spheres, represent silanol nest defects. (b) Slab model with the *z*-axis being perpendicular to the (101) plane of the DDR zeolite. The directions of the front and side views are displayed with respect to the top view. The bottom two figures are the front (*left*) and side (*right*) views of each model.

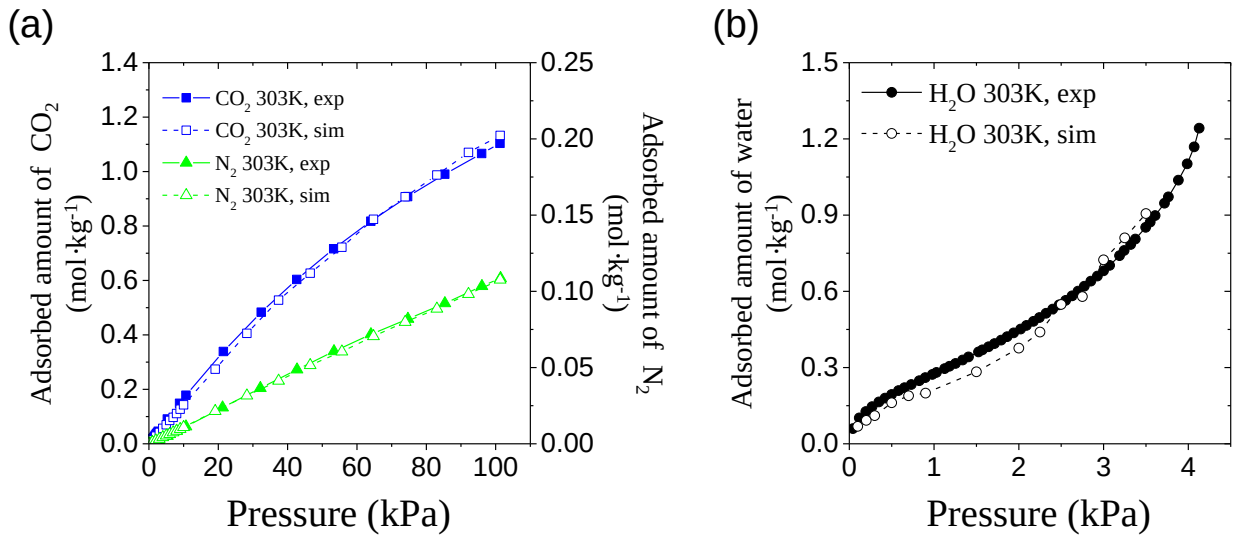

Fig. S14. Adsorption isotherms of (a) CO_2 (*square*) and N_2 (*triangle*) and (b) H_2O single components in DDR zeolites at 303 K, obtained from experiment (*filled* symbol)[1] and simulation (*open* symbol).

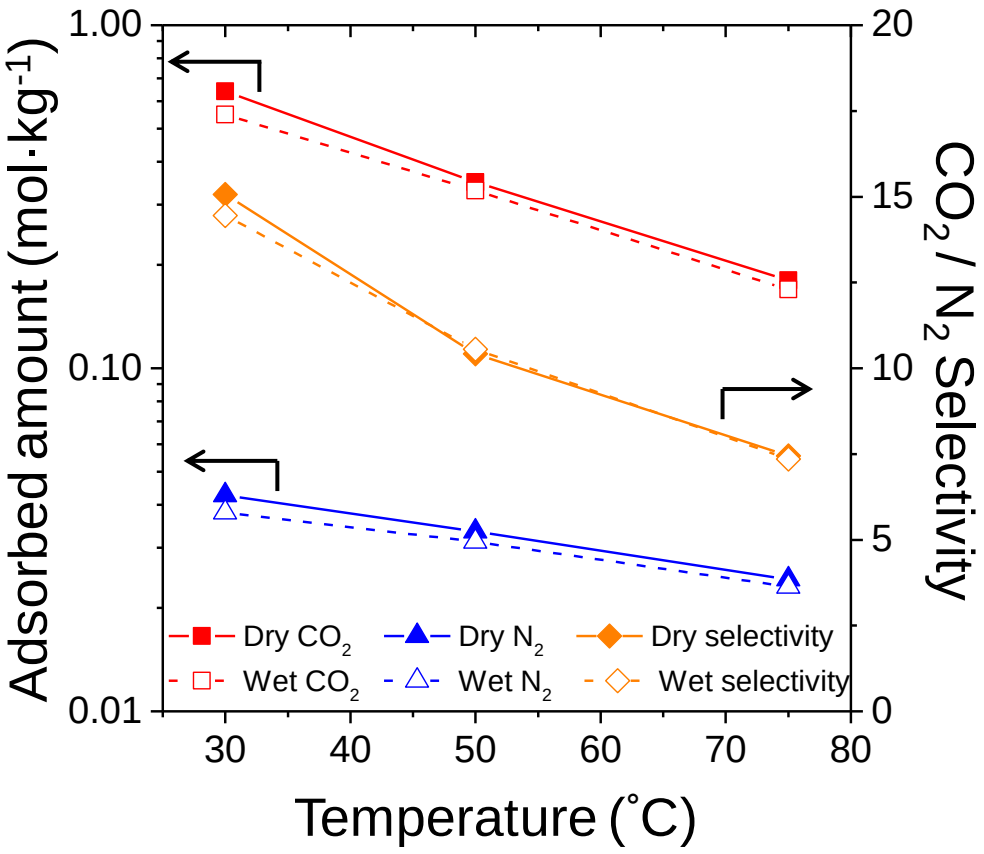

Fig. S15. Adsorbed amount of CO_2 and N_2 molecules and the corresponding CO_2/N_2 adsorption selectivity under the dry (50:50 DRY) and wet (50:50 WET) conditions obtained from both experiments and simulations (based on the model shown in Fig. S13a). Three temperatures (30, 50, and 75 ℃), which are representative of the post-combustion carbon capture process, are considered. Lines are included as a visual guide. Closed symbol and solid line means the dry condition, and open symbol and dash line means the wet condition. Square and triangle symbol represent the adsorbed amounts of CO_2 and N_2, respectively. Diamond symbol shows adsorption selectivity.

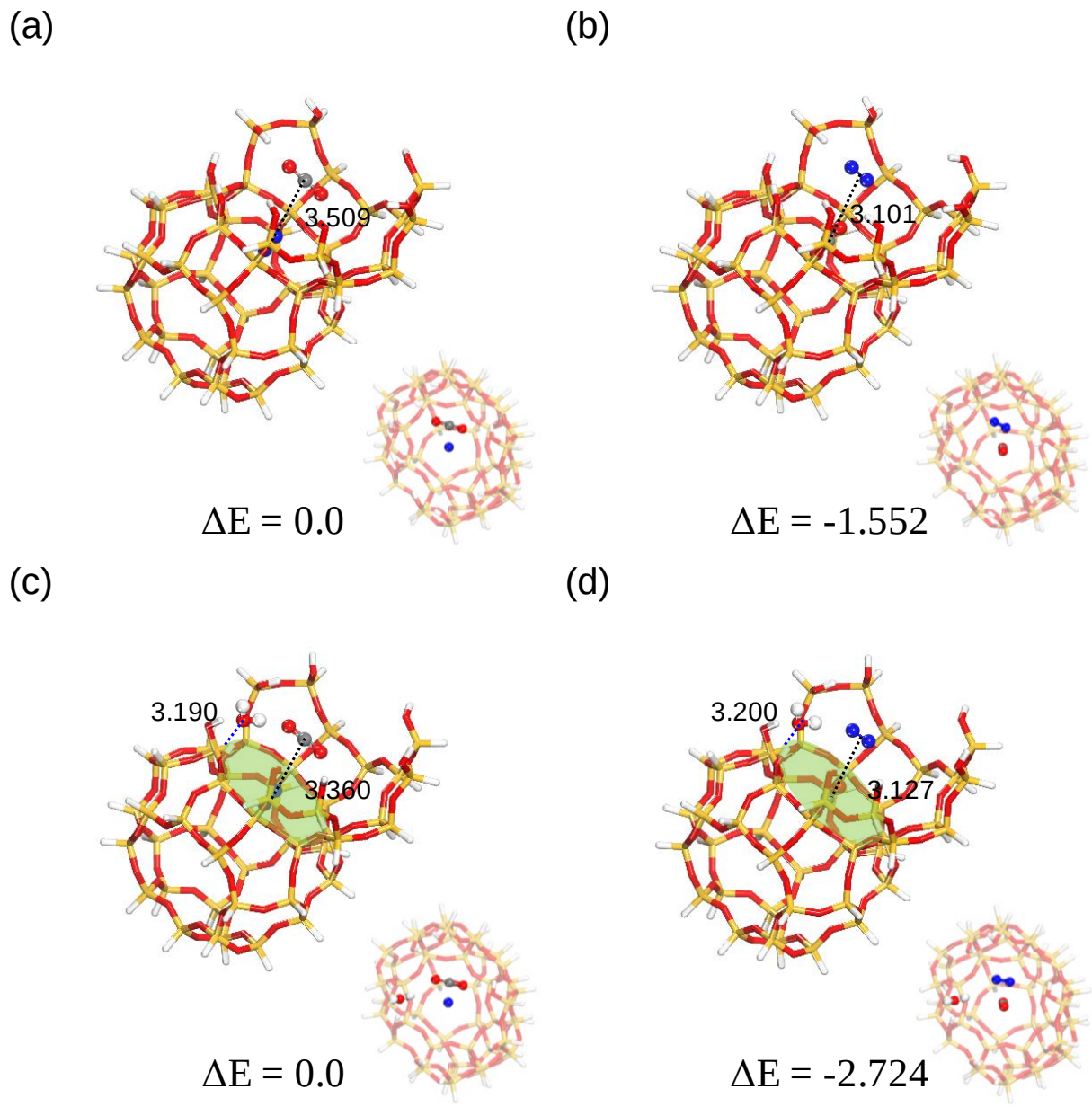

Fig. S16. DFT calculation results with the DDR 46T model under (a)-(b) dry (50:50 DRY) and (c)-(d) wet (50:50 WET) conditions. The configurations in (a) and (c) represent the feature that N_2 is located at a pore window and CO_2 is near the surface, while those in (b) and (d) represent the feature that CO_2 is located at a pore window and N_2 is near the surface. The numbers next to the figure in (b) and (d) indicate the energy in kcal·mol^{-1} relative to those shown in (a) and (c), respectively. The method used for calculating energies and color scheme are identical to those for Fig. 4.

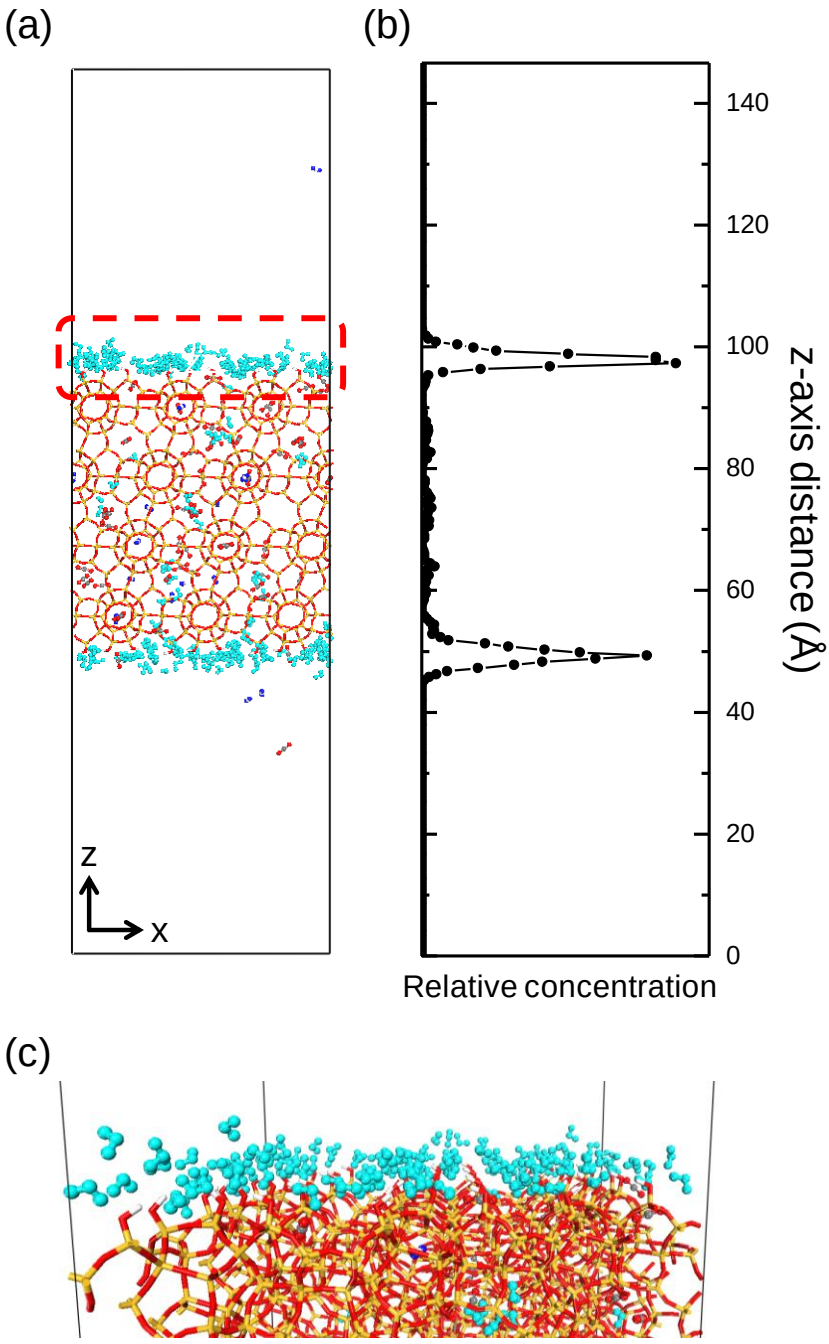

Fig. S17. (a) Most stable configuration of adsorbed molecules on the slab model (shown in Fig. S13b) at 303 K under the wet condition (50:50 WET). Cyan molecules represent adsorbed water on surface silanol and a red dashed box designates the surface region in the slab model. (b) Relative concentration profile of water along the z-axis. (c) Enlarged snap-shot of the surface region displayed in (a).

Table S1. Contact angle of a water droplet on membranes DZ.

Sample.	Contact angle of a water droplet (°)
DZ_2d	8
DZ_4d	62
DZ_6d	69
DZ_8d	87
DZ_10d	95

Table S2. Thickness of membrane DZ series estimated from the corresponding cross-sectional SEM images.

Sample.	Thickness (μm)
DZ_4d	3.9 ± 0.1
DZ_6d	3.90 ± 0.8
DZ_8d	5.3 ± 0.3
DZ_10d	7.2 ± 0.1
DZ_15d	7.8 ± 1.1

Table S3. Summary of potential parameters and partial charges used in the GCMC simulation. The functional form for the Lennard-Jones potential is $E = D_0\left[\left(\frac{R_0}{R}\right)^{12} - 2\left(\frac{R_0}{R}\right)^{6}\right]$ and that for coulombic potential is $E = C\frac{q_1 q_2}{\varepsilon R}$, where C = 332.0647/(kcal/mol)Å /e^2 is a unit conversion factor.

Atom	charge	Atom – Atom		Atom – $O_{zeolite}$	
		D_0 (kcal/mol)	R_0 (Å)	D_0 (kcal/mol)	R_0 (Å)
$Si_{zeolite}$	2.05	-	-	-	-
$O_{zeolite}$	-1.025	-	-	-	-
$O_{silanol}$	-0.95	0.1554	3.5532	-	-
$H_{silanol}$	0.4375	-	-	-	-
C (CO_2)	0.6512	0.05589710	3.09462787	0.09975593	2.80991537
O (CO_2)	-0.3256	0.15998110	3.40442739	0.16877035	3.27702795
N (N_2)	-0.40484	0.07233299	3.72657400	0.11575265	3.50342855
d_{N2}	0.80968	-	-	-	-
O (H_2O)	-0.834	0.1514456	3.5377082	0.16273953	3.62517453
H (H_2O)	0.417	-	-	-	-

References

1. E. Kim, K. Lim, T. Lee, K.-S. Ha, D.-Y. Han, J. Nam, N. Choi, I.-J. Cho, A.C.K. Yip, J. Choi, *Chem. Eng. J.*, 2016, **306**, 876-888.
2. Z. Zhou, S. Nair, US 2013/0064747 A1, 2013.
3. Z. Lai, G. Bonilla, I. Diaz, J.G. Nery, K. Sujaoti, M.A. Amat, E. Kokkoli, O. Terasaki, R.W. Thompson, M. Tsapatsis, D.G. Vlachos, *Science*, 2003, **300**, 456-460.
4. K. Ha, Y.J. Lee, H.J. Lee, K.B. Yoon, *Adv. Mater.*, 2000, **12**, 1114-1117.
5. J.S. Lee, K. Ha, Y.J. Lee, K.B. Yoon, *Adv. Mater.*, 2005, **17**, 837-841.
6. E. Kim, W. Cai, H. Baik, J. Choi, *Angew. Chem., Int. Ed.* , 2013, **52**, 5280-5284.
7. E. Kim, W. Cai, H. Baik, J. Nam, J. Choi, *Chem. Commun.*, 2013, **49**, 7418-7420.
8. E.W. Valyocsik, EU No. 0195498A2, 1986.
9. J. Kuhn, J. Gascon, J. Gross, F. Kapteijn, *Micropor. Mesopor. Mater.*, 2009, **120**, 12-18.
10. T. Lee, J. Choi, M. Tsapatsis, *J. Membr. Sci.*, 2013, **436**, 79-89.
11. E. Kim, T. Lee, H. Kim, W.J. Jung, D.Y. Han, H. Baik, N. Choi, J. Choi, *Environ. Sci. Technol.*, 2014, **48**, 14828-14836.
12. http://accelrys.com/products/materials-studio/index.html.
13. R. Krishna, J.M. van Baten, *Langmuir*, 2010, **26**, 2975-2978.
14. J.G. Harris, K.H. Yung, *J. Phys. Chem.*, 1995, **99**, 12021-12024.
15. C.S. Murthy, K. Singer, M.L. Klein, I.R. McDonald, *Mol. Phys.*, 1980, **41**, 1387-1399.
16. K. Makrodimitris, G.K. Papadopoulos, D.N. Theodorou, *J. Phys. Chem. B*, 2001, **105**, 777-788.
17. W.L. Jorgensen, J. Chandrasekhar, J.D. Madura, R.W. Impey, M.L. Klein, *J. Chem. Phys.*, 1983, **79**, 926-935.
18. R. Krishna, J.M. van Baten, *Sep. Purif. Technol.*, 2008, **61**, 414-423.
19. R. Krishna, J.M. van Baten, *Micropor. Mesopor. Mater.*, 2008, **109**, 91-108.
20. R. Krishna, J.M. van Baten, *J. Membr. Sci.*, 2010, **360**, 323-333.
21. R. Krishna, J.M. van Baten, *Langmuir*, 2010, **26**, 10854-10867.
22. J.C. Crabtree, M. Molinari, S.C. Parker, J.A. Purton, *J. Phys. Chem. C*, 2013, **117**, 21778-21787.
23. S. Himeno, M. Takenaka, S. Shimura, *Mol. Simul.*, 2008, **34**, 1329-1336.
24. J. Yang, J. Li, W. Wang, L. Li, J. Li, *Ind. Eng. Chem. Res.*, 2013, **52**, 17856-17864.
25. J. Kuhn, J.M. Castillo-Sanchez, J. Gascon, S. Calero, D. Dubbeldam, T.J.H. Vlugt, F. Kapteijn, J. Gross, *J. Phys. Chem. C*, 2009, **113**, 14290-14301.
26. R. Krishna, *Phys. Chem. Chem. Phys.*, 2015, **17**, 39-59.
27. Y.G. Bushuev, G. Sastre, *J. Phys. Chem. C*, 2009, **113**, 10877-10886.
28. M. Trzpit, M. Soulard, J. Patarin, N. Desbiens, F. Cailliez, A. Boutin, I. Demachy, A.H. Fuchs, *Langmuir*, 2007, **23**, 10131-10139.
29. A. Özgür Yazaydın, R.W. Thompson, *Micropor. Mesopor. Mater.*, 2009, **123**, 169-176.
30. G. Barone, N. Armata, A. Prestianni, T. Rubino, D. Duca, D.Y. Murzin, *J. Chem. Theory Comput.* , 2009, **5**.
31. V. Shapovalov, A.T. Bell, *J. Phys. Chem. C* 2010, **114**, 17753-17760.
32. B. Delley, *J. Chem. Phys.*, 1990, **92**, 508-517.
33. B. Delley, *J. Chem. Phys.*, 2000, **113**, 7756-7764.
34. A. Tkatchenko, M. Scheffler, *Phys. Rev. Lett.*, 2009, **102**, 073005.
35. B. Delley, *Mol. Simul.*, 2006, **32**, 117-123.